Out-of-Plane Measurements of the Structure Functions of the Deuteron

G.P.Gilfoyle

Physics Department, University of Richmond, VA, 23173 USA

W.K.Brooks, B.A.Mecking

Thomas Jefferson National Accelerator Facility, 12000 Jefferson Avenue, Newport News, VA 23606, USA

S.Kuhn, L.Weinstein

Physics Department, Old Dominion University, Norfolk, VA, 23529, USA

M.F.Vineyard

Physics Department, Union College, Schenectady, New York, 12308 USA

Abstract

We propose the measurement of the structure functions of the deuteron f'_{LT}, f_{TT}, and f_{LT} using the reaction $d(\vec{e}, e'p)n$ with CLAS. The 'standard model' of nuclear physics is not well-developed in the GeV region, and the relative importance of relativistic corrections, final-state interactions, meson-exchange currents, and isobar configurations is unknown. These data will provide a baseline for conventional nuclear physics, so deviations from the model at higher Q^2 can be attributed to quark-gluon effects with greater confidence. The three structure functions will be extracted by measuring different moments of the out-of-plane production in CLAS. Each of these moments is related to a different asymmetry which is, in turn, proportional to a particular structure function. The structure function f'_{LT} is nonzero only in the out-of-plane production. This analysis will be performed on the existing E5 data set that covers the range $Q^2 = 0.2 - 5.0$ $(\mathrm{GeV/c})^2$. We will study the reaction in quasi-elastic kinematics first and later investigate higher energy transfers. Our preliminary results show we can observe small asymmetries with good precision in quasi-elastic kinematics.

1 Introduction

We propose to analyze existing CLAS data from the E5 running period to extract the structure functions f_{LT}, f_{TT}, and f'_{LT} of the deuteron using the proton azimuthal distribution from the $d(\vec{e}, e'p)n$ reaction. Electron scattering from the deuteron is an essential testing ground for any model of the nucleon-nucleon force. It is the simplest nucleus in nature and the electromagnetic interaction is well-known and weak (so it can be treated in first-order perturbation theory). The structure functions describing the electromagnetic response of nuclei are sensitive to a variety of phenomena depending on the choice of kinematics, *i.e.* the energy transfer ν and the 4-momentum transfer Q^2. Using a polarized beam and the large acceptance of the CLAS detector we will break new ground in the investigation of the structure function f'_{LT} which is non-zero only for the out-of-plane production. This analysis will focus on the quasi-elastic regime first to study the Q^2 evolution of the structure functions from the better-known, low-Q^2 region where data now exist up to the GeV region where there are few measurements and our theoretical understanding is incomplete. The quasi-elastic structure functions are also less sensitive to some of the non-nucleonic degrees-of-freedom so they serve as a benchmark for other kinematic regions. We will later push this study beyond the quasi-elastic region to higher energy transfers.

Understanding the deuteron tests the 'standard' or hadronic model of nuclear physics. The goal is to construct a 'consistent and exact description' of few-body nuclei (^{2}H, ^{3}H, ^{3}He, ^{4}He) [1]. For example, it is an open question whether a single interaction or current operator can account for the attributes of all these nuclei. Calculations using hadronic effects like meson-exchange currents (MEC), isobar configurations (IC), and final-state interactions (FSI) are under development, but have yet to be fully challenged by data in the GeV region [1, 2]. The influence of relativity is also being studied [1, 2, 3, 4, 5]. Previous results at lower Q^2 reveal the onset of many of these effects so a complete, modern calculation is needed to compare with data across the full range of Q^2 to test and understand the hadronic model in this region. It is worth mentioning these issues were raised as 'Key Questions' at the Jefferson Laboratory PAC14 Few-Body Workshop [1].

Of equal importance is finding where and how the 'standard model' of nuclear physics breaks down; requiring quark-gluon or quark and flux-tube degrees-of-freedom. Studying this transition is an essential goal of nuclear physics [1, 7]. The basic idea is that if we cannot describe observations with all of the pieces mentioned above, then we would see genuine quark effects in the nucleus. Clearly, we cannot make that leap without getting firm control of the calculations using the hadronic degrees-of-freedom. It is expected that transition will occur in the GeV region [2, 7].

Out-of-plane measurements probe components of the electromagnetic response of the deuteron that are difficult or impossible to investigate otherwise. The deuteron's electromagnetic structure is studied via electron scattering which is characterized by a set of response functions that connect model calculations and measurements. Typically, (*i.e.*, with unpolarized targets and detectors that all lie in the scattering plane), there are four response functions determined by different combinations of the longitudinal and transverse components of the electromagnetic current. However, with polarized electron beams and measurements of the ejected proton out of the scattering plane of the electron, a new response function can be measured. This fifth response function f'_{LT} is the imaginary part of the interference between the longitudinal and transverse parts of the electromagnetic current. The same experimental capabilities can also separate the longitudinal-transverse response function f_{LT} and the transverse-transverse response function f_{TT} [8]. The influence of different phenomena (*e.g.*, relativity, FSI, *etc.*) varies with the each of the structure functions and depends on the choice of kinematics. For example, f'_{LT} is more sensitive to relativistic corrections than f_{TT}, but this sensitivity declines in the dip region. Measuring the out-of-plane behavior is a tool for unraveling the deuteron's electromagnetic response. Progress in making these sorts of measurements has required rather substantial efforts and, as a consequence, produced limited data sets. The CLAS detector is inherently an out-of-plane detector and is ideally suited for studying the out-of-plane behavior of the electromagnetic structure functions of the deuteron.

We propose here to analyze already-collected data of the $d(\vec{e}, e'p)n$ reaction from the CLAS E5 running period. About 2.3 billion triggers were collected during this run period in the range $Q^2 = 0.2 - 5.0$ $(\mathrm{GeV/c})^2$ using a dual-cell target containing deuterium (as the primary target) and hydrogen (for *in situ* calibrations). Three sets of run conditions were used: 4.23 GeV with a normal torus field polarity, 2.56 GeV with a normal torus field polarity, and 2.56 GeV with a reversed torus field polarity to reach lower Q^2. Cooking of the data was completed in late 2002. We will extract three structure functions f_{LT}, f_{TT}, and f'_{LT} by studying the variation of the cross section on ϕ_{pq}, the angle between the scattering plane of the incoming and scattered electron and the reaction plane of the ejected proton and neutron. The kinematic range of the measurements will enable us to study the Q^2 evolution from the upper limit of most previous studies of these structure functions ($Q^2 \approx 0.2$ (GeV/c)^2) to a region where some models are expected to fail (at $Q^2 \approx 1.0$ (GeV/c)^2). These measurements will be compared with several different theoretical calculations.

Below, we develop the formalism used to analyze the electromagnetic response functions and discuss the current status of experiment and theory. We then show how CLAS will be used to make out-of-plane measurements and demonstrate the feasibility of those measurements. We then summarize our results.

2 Formalism for $d(e, e'p)X$

For the case of a polarized electron beam incident on an unpolarized target, the three-fold differential cross section can be written in the one-photon exchange approximation as

$$\begin{aligned} \frac{d^3\sigma}{d\nu d\Omega_e d\Omega_p} &= c\{\rho_L f_L + \rho_T f_T + \rho_{LT} f_{LT} \cos(\phi_{pq}) \\ &\quad + \rho_{TT} f_{TT} \cos(2\phi_{pq}) + h\rho'_{LT} f'_{LT} \sin(\phi_{pq})\} \end{aligned} \tag{1}$$

where

$$c = \frac{\alpha E'}{6\pi^2 Q^4 E} \quad , \tag{2}$$

α is the fine-structure constant, E and E' are the incoming and outgoing electron energies respectively, Q^2 is the square of the 4-momentum transfer, h is the electron beam helicity (± 1), the $\rho_{\lambda\lambda'}$ are the virtual-photon density matrix elements which depend only on the electron kinematics (see Reference [9]), and the $f_{\lambda\lambda'}$ are the response functions in the center of mass. The azimuthal angle ϕ_{pq} is the angle between the scattering plane defined by the incoming and outgoing electrons and the reaction plane defined by the ejected proton and neutron (see figure below). The response functions depend on the energy transfer ν, the 3-momentum

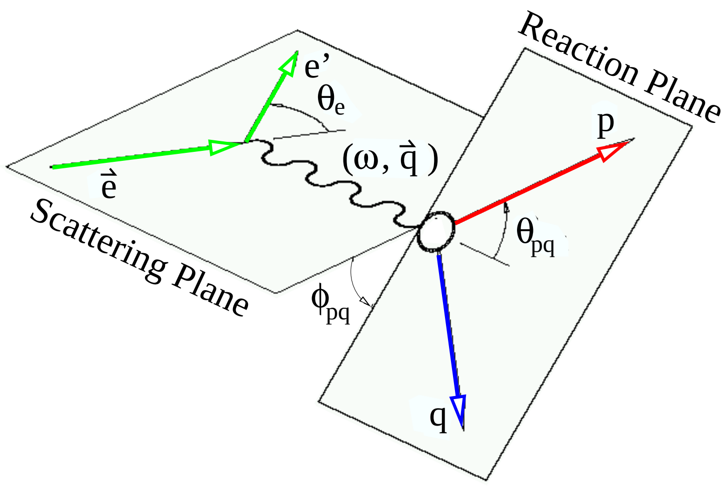

Figure 1: Kinematic quantities for $d(\vec{e}, e'p)n$.

transfer $\vec{q}$, and θ_{pq}^{cm} where θ_{pq}^{cm} is the angle between $\vec{q}$ and the ejected proton momentum in the center-of-mass frame. The missing momentum is often used to describe this reaction and is

$$\vec{p}_m = \vec{q} - \vec{p}_p \tag{3}$$

where $\vec{p}_p$ is the ejected proton momentum. In the plane-wave impulse approximation this missing momentum is the opposite of the initial momentum of the proton.

When using conventional, small-acceptance, spectrometers, one approaches the problem of extracting the response functions by constructing asymmetries to isolate different components. Consider the following asymmetries measured at azimuthal angle ϕ_{pq} around the $\vec{q}$ vector.

$$A_{LT} = \frac{\sigma_{0^\circ} - \sigma_{180^\circ}}{\sigma_{0^\circ} + \sigma_{180^\circ}} = \frac{\rho_{LT} f_{LT}}{\rho_L f_L + \rho_T f_T + \rho_{TT} f_{TT}} \tag{4}$$

$$A'_{LT} = \frac{\sigma_{90^\circ}^{(+1)} - \sigma_{90^\circ}^{(-1)}}{\sigma_{90^\circ}^{(+1)} + \sigma_{90^\circ}^{(-1)}} = \frac{\rho' f'_{LT}}{\rho_L f_L + \rho_T f_T - \rho_{TT} f_{TT}} \tag{5}$$

$$A_{TT} = \frac{\sigma_{0^\circ} + \sigma_{180^\circ} - 2\sigma_{90^\circ}}{\sigma_{0^\circ} + \sigma_{180^\circ} + 2\sigma_{90^\circ}} = \frac{\rho_{TT} f_{TT}}{\rho_L f_L + \rho_T f_T} \tag{6}$$

The subscripts refer to the value of ϕ_{pq} and the superscripts refer to the beam helicity. Note that in each case one divides by the sum of the measurements so that systematic uncertainties will be reduced. Each asymmetry is proportional to one of the response functions in Equation 1 so one can investigate the behavior of these terms in the cross section. One can combine Equations 4–6 and rearrange to get expressions for f_{LT}, f_{TT}, and f'_{LT}.

$$f_{LT} = \frac{\sigma_{0^\circ} - \sigma_{180^\circ}}{2c\rho_{LT}} \tag{7}$$

$$f'_{LT} = \frac{\sigma_{90^\circ}^{(+1)} - \sigma_{90^\circ}^{(-1)}}{2c\rho'_{LT}} \tag{8}$$

$$f_{TT} = \frac{\sigma_{0^\circ} + \sigma_{180^\circ} - 2\sigma_{90^\circ}}{4c\rho_{TT}} \tag{9}$$

These results (Equations 7–9) show how these response functions are determined from out-of-plane measurements with conventional spectrometers. Below we will discuss how to take advantage of the large acceptance of CLAS in making similar measurements.

3 Current Status

In this section we describe the world data for each of the three structure functions f'_{LT}, f_{TT}, and f_{LT}. We then show the relationship of this proposal to other Jefferson Lab experiments.

The measurements for f'_{LT} are sparse, but have given us a glimpse of the the physics to come. They require out-of-plane spectrometers and polarized beams. For quasi-elastic kinematics they have only been made at $Q^2 = 0.22~(\mathrm{GeV/c})^2$ and $Q^2 = 0.13~(\mathrm{GeV/c})^2$ at Bates [8, 10, 11]. The results are shown in Figure 2. That work demonstrated the utility of out-of-plane measurements and the calculations presented show that relativity already plays a significant role even at this low value of Q^2 [5]. In the right-hand panel of Figure 2, the solid curve includes relativistic corrections and is noticeably different from the other curves. The effect of final-state interactions is dramatic and can be seen in the left-hand panel of Figure 2. The double-dot-dashed line at $f'_{Lt} = 0$ is from a Plane-Wave Born Approximation calculation which does not include FSI. In general, f'_{LT} is non-zero only in the presence of final-state interactions. The other calculations do include FSI and they are all significantly different from zero. Unfortunately, the large uncertainties of the data prevent one from distinguishing among different effects like MEC, FSI, and IC or between different potentials. The calculations in Reference [10] (left-hand panel of Figure 2) by Arenhövel at $Q^2 = 0.13~(\mathrm{GeV/c})^2$ employed four different potentials and include effects from MEC, Δ-isobar contributions (IC), and relativistic corrections (RC). The calculations were insensitive to MEC and IC, but relativistic corrections make a noticeable contribution; about the same effect as the difference between different potentials. The calculations at $Q^2 = 0.22~(\mathrm{GeV/c})^2$ (right-hand panel of Figure 2) display a similar behavior. These studies have revealed the importance of relativity and FSI in this region of Q^2. The success of the Bates work at low Q^2 is an invitation to extend the measurements with CLAS. CLAS is an out-of-plane detector by its very nature so the analysis of the E5 data will dramatically improve the state-of-the-art of these measurements.

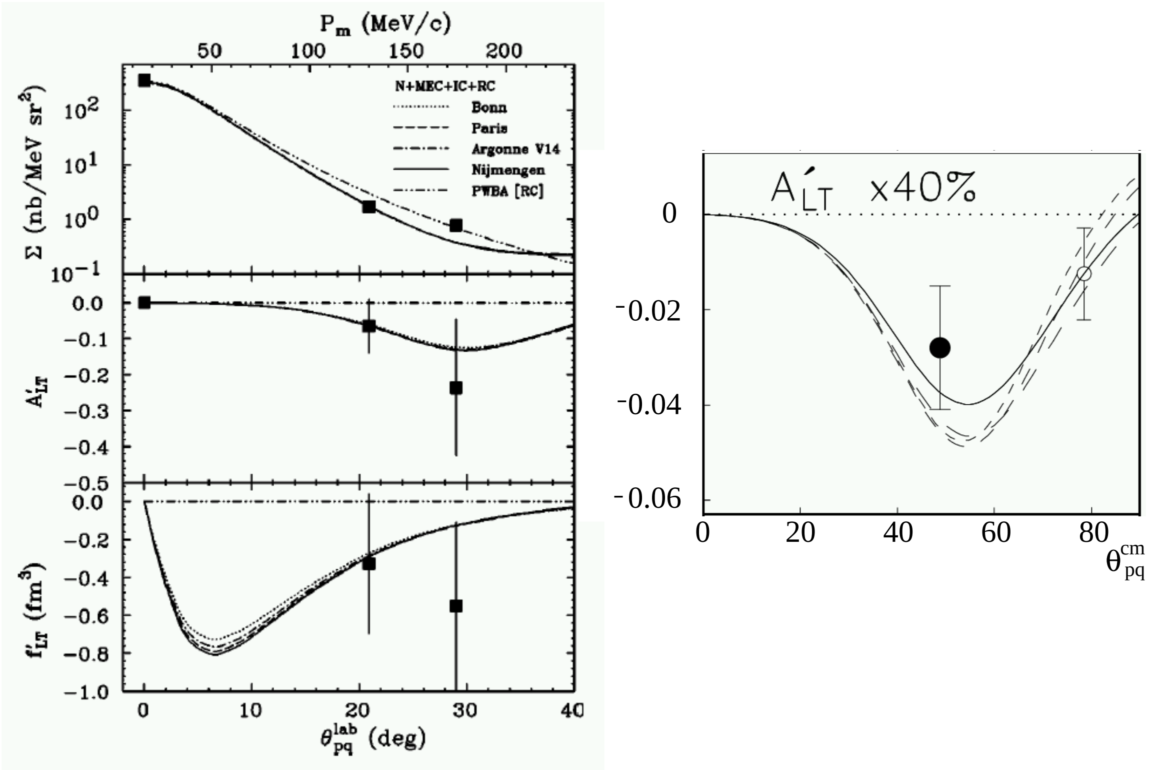

Figure 2: Measurements of f'_{LT} and its associated cross section and asymmetry from Reference [10] at $Q^2 = 0.13$ (GeV/c)^2 (left-hand panel) and A'_{LT} from Reference [8] at $Q^2 = 0.22$ (GeV/c)^2 (right-hand panel). The observations in the left-hand panel are shown as a function of θ_{pq}^{lab} in degrees and the ones in the right-hand panel are shown as a function of θ_{pq}^{cm} in degrees. The open circle is for anticipated data.

The situation is little different for observations of the transverse-transverse interference term f_{TT} in quasi-elastic kinematics. These experiments require out-of-plane measurements and unpolarized beam, but this portion of the cross section must be separated from the larger contributions of f_L, f_T, and f_{LT}. Three measurements have been made at Tohoku ($Q^2 = 0.013$ (GeV/c)^2), NIKHEF ($Q^2 = 0.21$ (GeV/c)^2), and Bates ($Q^2 = 0.22$ (GeV/c)^2) [8, 12, 13]. The lowest Q^2 measurements agree with a non-relativistic calculation which uses the Paris potential and includes the effect of MEC and IC, but the data have large uncertainties. The NIKHEF experiment could only put an upper limit on the structure function because it was combined with the larger longitudinal structure function f_L. The Bates results have smaller uncertainties than in the f'_{LT} case (see Figure 3 and compare with Figure 2), but one still cannot distinguish among MEC, FSI, RC, and IC effects. There is a clear need here to reduce the uncertainties and extend the measurements out to larger θ_{pq}^{cm} where the calculations diverge. Again, because of the considerable out-of-plane capabilities of CLAS we expect to significantly improve the state-of-the-art of these measurements.

The longitudinal-transverse interference structure function f_{LT} has been measured several times and with greater precision than the other two structure functions above. At the lowest $Q^2 = 0.013$ (GeV/c)^2 the data are reproduced by a non-relativistic calculation while at the highest ($Q^2 = 1.2$ (GeV/c)^2) the relativistic calculations of the asymmetry are preferred [12, 14]. Between these two extremes, the situation is less clear. At $Q^2 = 0.15$ (GeV/c)^2 data from NIKHEF were compared with calculations by Hummel and Tjon which include RC and FSI and calculations by Arenhövel that are non-relativistic but include MEC, IC, and FSI [13, 15, 16, 17]. The results for the combined f_L and f_{TT} structure function could not discriminate between the two calculations, but the results for f_{LT} favored the relativistic calculation of Hummel and

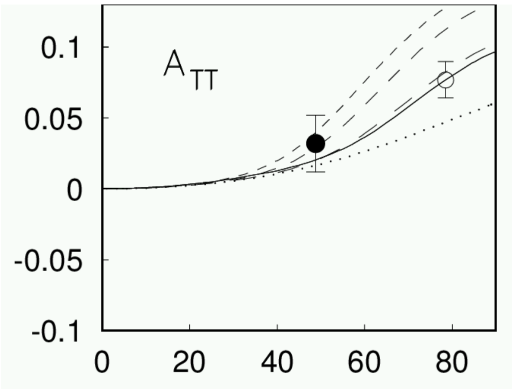

Figure 3: Measurements of f_{TT} as a function of θ_{pq}^{cm} for quasi-elastic kinematics from Reference [8]. The filled circle is the data, the open circle shows expected future results

Tjon. Measurements of f_{LT} at similar Q^2 at Bates and Saclay agree better with non-relativistic calculations by Arenhövel than with the same relativistically corrected ones [18, 19]. The Arenhövel calculations include MEC in the Saclay work and MEC, FSI, and IC in the Bates experiment. In the Saclay work, there is a 'disconcerting' spread among the relativistic calculations suggesting the need to improve these calculations by performing experiments at higher Q^2 [19]. A nearby measurement at $Q^2 = 0.145\ (\mathrm{GeV/c})^2$ clearly favors the inclusion of relativity [20]. It is worth noting that a recent measurement of the cross section in the middle of this region ($Q^2 = 0.67\ (\mathrm{GeV/c})^2$) was reproduced with a calculation by Arenhövel that includes relativistic effects, FSI, MEC, and IC [21, 22]. The E5 data spans the Q^2 range of the observations discussed here so this analysis project holds the promise of connecting the picture of the deuteron at low Q^2 to high Q^2. In addition, the E5 data have considerable overlaps and consistency checks among the three sets of run conditions.

As one moves away from the quasi-elastic region the mixture of physics effects changes. The data show an increased sensitivity to MEC and IC effects for f_{TT} in the dip and Δ regions and are not influenced by RC or FSI [8, 23]. The other structure functions f_{LT} and f'_{LT} are the opposite; sensitive to RC and FSI effects and independent of MEC and IC. Unfortunately, the data are sparse and often have large uncertainties.

In summary, several points can be made about our current understanding of the deuteron structure functions. First, different structure functions are influenced by different physics. The f_{LT} and f'_{LT} structure functions are sensitive to relativistic effects and f'_{LT} is especially sensitive to final state interactions. The other structure function in our study, f_{TT}, is more sensitive to non-nucleonic degrees of freedom (MEC and IC). Second, the different kinematic regimes probe different physics. On the quasi-elastic ridge, MEC and IC contribute little, but their effect increases as one moves into the dip and Δ regions while the impact of RC and FSI declines. Finally, there is little data in the range $Q^2 = 0.2 - 1.0\ (\mathrm{GeV/c})^2$ where it is needed to unravel all of the competing effects mentioned above.

This analysis project will complement other experiments at Jefferson Lab. Experiment E02-101 (K. Wang spokesperson and contact) is designed to extract all the structure functions f_L, f_T, f_{LT}, f_{TT}, and f'_{LT} at threshold for $Q^2 = 0.47\ (\mathrm{GeV/c})^2$ using the HRS and BigBite spectrometers in Hall A. Threshold kinematics have been chosen to minimize the contribution of nucleonic effects to study the effects of RC, MEC, and IC. Our study of quasi-elastic effects reduces the influence of non-nucleonic degrees of freedom (MEC and IC) so we are exploring different physics. In addition, E02-101 will take data at a single Q^2 while the CLAS data cover a larger kinematic region. Figure 4 displays a comparison of the kinematic coverage of E01-020 and this analysis. The red, green, and blue areas show the kinematic coverage for the three sets of run conditions for the E5 run period. The square is the proposed kinematics for E02-101. The quasi-elastic ridge can be clearly seen along the low-ν edge of the E5 kinematics. There is also a large amount of data at higher ν or W that will be analyzed.

Experiment E01-020 has two parts made up of two previous proposals: PR-01-007 (formerly E94-004, W.Boeglin spokesperson and contact) and PR-01-008 (P.Ulmer spokesperson and contact). Data collection

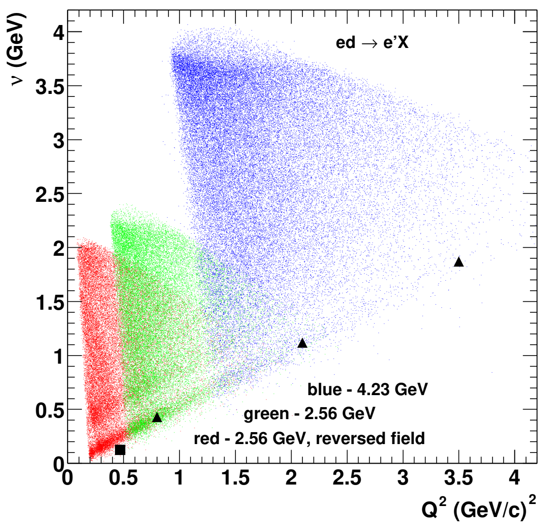

Figure 4: Energy loss of the electron versus Q^2. The red, green, and blues areas represent the kinematic coverage for the three running conditions during the E5 run period. The triangles are the kinematics for the measurement of σ_{LT} for E01-020. The square is the anticipated kinematics for E02-101.

for this experiment was completed in fall, 2002 in Hall A. In the first part (the former E94-004) parallel and anti-parallel kinematics will be used to study the short-range structure of the deuteron. Perpendicular kinematics at the quasi-elastic peak will be used to extract f_{LT} at $Q^2 = 0.8$, 2.1, and 3.5 $(\mathrm{GeV/c})^2$. The measurement of f_{LT} in this experiment overlaps with our proposed analysis project. However, we will be able to extract f_{TT} and f'_{LT} using our out-of-plane measurements. The CLAS detector has lower resolution, but greater kinematic coverage so the two experiments will provide a cross-check for each other. See Figure 4 for a comparison of the kinematics of E01-020 with this analysis.

In the second part of E01-020, the angular distribution of the quasi-elastic peak will be measured at the same values of Q^2 and with recoil momenta between 0.2 GeV/c and 0.5 GeV$/c$. The goal is to study FSI and non-nucleonic degrees of freedom (MEC and IC). The measurements will be entirely in the scattering plane. The kinematic region overlaps with the CLAS data of this proposed analysis, but no effort will be made to extract the structure functions.

To summarize, the analysis of the E5 data to extract the structure functions in the range $Q^2 = 0.2 - 5.0$ $(\mathrm{GeV/c})^2$ from the out-of-plane data will explore new territory. The world's data for f'_{LT} and f_{TT} are sparse and few exist in the Q^2 range covered here. There are more measurements of f_{LT}, but the interpretation of the results is inconsistent which may mean that our understanding of the deuteron is incomplete. The new measurements proposed here are in a Q^2 region where the onset of relativistic effects is increasingly important and contradictory results exist from past work. A systematic study of the out-of-plane structure functions across a wide range in Q^2 will shed light on this problem. The precision of the data may also permit the study of other effects like MEC and IC. The analysis will also complement other experiments at Jefferson Lab to study the deuteron.

4 Measuring Response Functions with CLAS

4.1 Introduction

In this section we discuss our preliminary results and show that the proposed analysis project is feasible. We have measured A'_{LT} on a subset of the E5 data and demonstrated that we can extract this small deuteron structure function with adequate precision to evaluate the success of different theoretical models. The analysis here is restricted to the quasi-elastic peak so we can compare our results to previous measurements at Bates at lower Q^2. The theoretical description of the deuteron structure functions is simpler for quasi-elastic kinematics because contributions from meson-exchange currents (MEC) and isobar configurations (IC) are expected to be smaller [10]. In this section we will discuss data selection and corrections, extracting A'_{LT} with different methods, and present some preliminary results.

4.2 Data Selection and Corrections

We are investigating the $d(\vec{e}, e'p)n$ reaction by detecting the scattered electron and the ejected proton with CLAS and using missing mass to identify the neutron. The data were collected during the E5 run period (Spring, 2000) and consist of runs 24020–24588. About 2.3 billion triggers were collected under three sets of run conditions: (1) $E_{beam} = 4.23$ GeV, $I_{torus} = 3375$ A, normal polarity (inbending electrons), (2) $E_{beam} = 2.56$ GeV, $I_{torus} = 2250$ A, normal polarity, and (3) $E_{beam} = 2.56$ GeV, $I_{torus} = 2250$ A, reversed polarity (outbending electrons) to reach lower Q^2. Electrons were identified as negative tracks from the EVNT bank (produced by SEB) in coincidence with hits in the Cerenkov counters, the TOF scintillators, and the electromagnetic calorimeter. A cut on the number of photo-electrons of greater than 2.5 from the Cerenkov counters was imposed to reduce the number of negative pions misidentified as electrons [24]. Protons were taken from the EVNT bank. Figure 4 above shows the two-dimensional distribution of the energy loss of the electron versus Q^2. The large kinematic coverage can be seen as well as the extensive overlaps between the different data sets. These overlaps will provide cross checks on the analysis. The acceptance of CLAS for ep coincidences is, on average, 20-30%. Figure 5 shows the missing mass versus θ_{pq}^{cm} for the 2.6 GeV, reversed field (left panel) and 4.2 GeV, normal field (right panel) running conditions. The

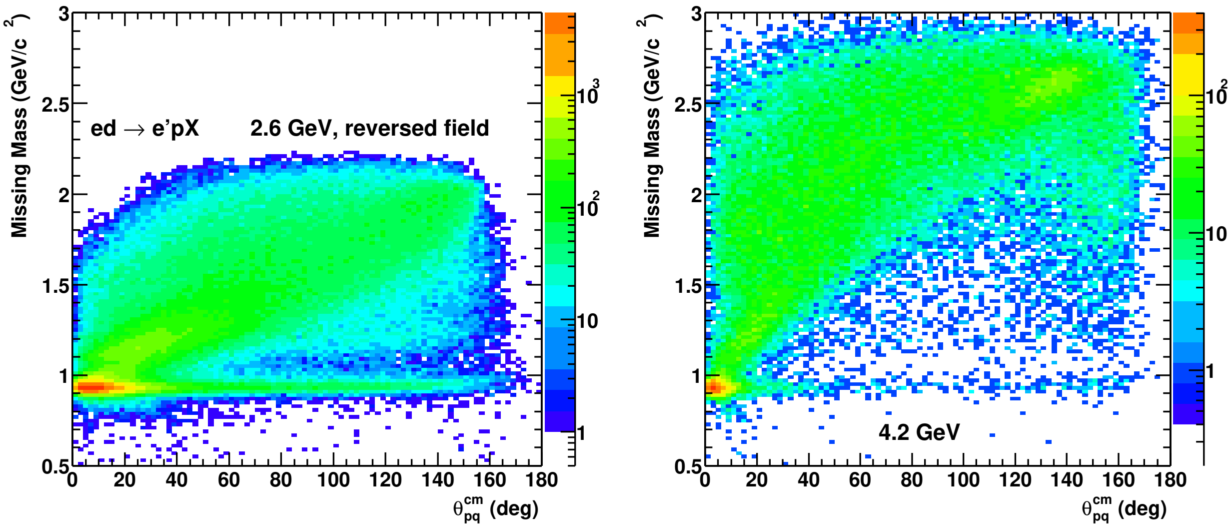

Figure 5: Missing mass versus θ_{pq}^{cm} for $ed \rightarrow e'pX$ for 2.6 GeV, reversed field (left panel) and 4.2 GeV (right panel).

ridge at the missing mass of the neutron (0.94 GeV) is clearly visible, well separated, and extends to large angle especially for the 2.6 GeV, reversed field data. We will be able to identify the missing neutron across the full kinematic range.

Momentum corrections have not yet been applied to the events analyzed here because we have found those corrections to have little effect on the results [25, 26]. In Reference [25] the neutron mass determined from the missing mass technique for the reaction $p(e, e'\pi^+)X$ was 0.93490 ± 0.00003 GeV/c^2 before applying corrections and only increased to 0.93570 ± 0.00003 GeV/c^2 after corrections. We will apply these corrections later. The method used is described in CLAS-NOTE 2001-18.

Vertex cuts were imposed on the electron and proton tracks so only events coming from the central part of the deuterium or proton target would be analyzed. Figure 6 shows the distribution of the z component of the electron vertex for a single data file from run 24029. The red lines are at the limits of the vertex cut for the deuteron target and the proton target.

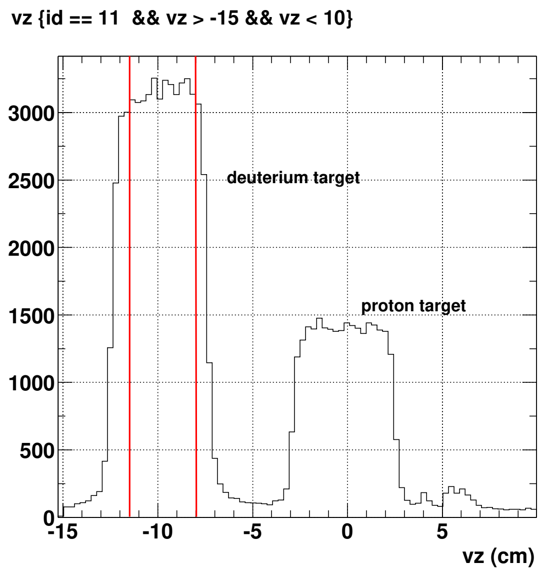

Figure 6: Distribution of the z component of the electron vertex. Red lines represent cuts imposed on all good events.

To account for any difference in the amount of beam striking the target for the two helicities we determined the beam charge asymmetry for each set of running conditions and then corrected our data for it. The beam charge asymmetry (BCA) is defined as the ratio of the normalized beam intensities for the two different beam helicities. We calculated the beam charge asymmetry using the inclusive (e, e') electron yields for positive (N_+) and negative (N_-) helicities with the following expression.

$$A_Q = \frac{N_+}{N_-} \tag{10}$$

The inclusive cross section has no helicity dependence and is more reliable than the Faraday cup readings [27]. Some of our results are shown below in Figure 7 for the 2.56-GeV, normal-torus-polarity running conditions. The average for these run conditions is $A_Q = 0.9952 \pm 0.0007$. The half-wave plate which determines the beam helicity was fixed during the E5 run period. This means we should see not shifts in the BCA, which is consistent with Figure 7.

The measurements of the $d(\vec{e}, e'p)n$ reaction in this proposed analysis are subject to radiative corrections. We are using a modified version of the program EXCLURAD written by Afanasev, *et al.* to perform those calculations [28]. This code applies a more sophisticated method than the usual approach of Mo and Tsai or Schwinger and takes into account the exclusive nature of our measurements [29, 30]. We have not yet applied those corrections to our data, but we have revised EXCLURAD so that it can be applied to these data. The code was originally written for the $p(e, e'\pi^+)X$ reaction and we have modified it for the $d(\vec{e}, e'p)n$ reaction. Some of this work is described in the Appendix.

4.3 Extracting Asymmetries

In this section we discuss several methods for extracting the asymmetries A'_{LT}, A_{LT}, and A_{TT} as defined in Equations 4-6. The first uses small angle bins to directly apply Equations 4-6 to the data and calculate all three asymmetries. The second method is based on calculating different moments of the data and takes

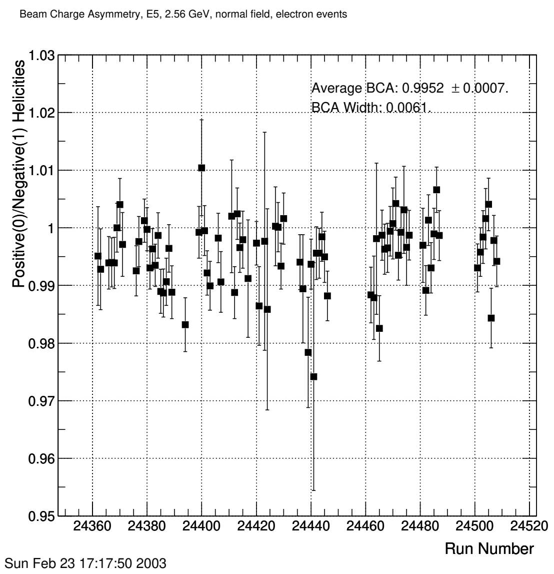

Figure 7: Beam charge asymmetry (BCA) for the 2.56-GeV, normal-torus-field-polarity running conditions.

advantage of the full angular coverage of CLAS to extract the three asymmetries. The third technique fits the out-of-plane angular distribution of the asymmetry and should yield the same results as the previous method for A'_{LT}, but does not apply to A_{LT} and A_{TT}.

The results from applying Equations 4-6 using small ($\pm 4^\circ$) angle bins around $\phi_{pq} = 90^\circ$ and $\phi_{pq} = 180^\circ$ are shown in the Figure 8 below. The results for A_{LT} show a large, negative asymmetry for $\theta_{pq}^{cm} < 30^\circ$ which decreases at larger angles where the uncertainties become significant. For A'_{LT} there is a small ($\approx 2\sigma$) excursion from zero in the range $\theta_{pq}^{cm} = 20^\circ - 30^\circ$ and the results are consistent with zero elsewhere. Note that the uncertainties are large on A'_{LT} which is expected to be small. The results for A_{TT} show a small, but significant asymmetry (about $4 - 5\sigma$) in the range $\theta_{pq}^{cm} = 0^\circ - 10^\circ$ which declines at larger angles.

We now develop the method to extract the asymmetries using the moments of the full ϕ_{pq} distribution measured with CLAS. The triply differential cross section for $d(\vec{e}, e'p)n$ can be written as

$$\frac{d^3\sigma}{d\nu d\Omega_e d\Omega_p} = \sigma^{\pm} = c[\rho_L f_L + \rho_T f_T + \rho_{LT} f_{LT} \cos(\phi_{pq}) + \rho_{TT} f_{TT} \cos(2\phi_{pq}) + h\rho'_{LT} f'_{LT} \sin(\phi_{pq})] \quad (11)$$

$$= \sigma_L + \sigma_T + \sigma_{LT} \cos\phi_{pq} + \sigma_{TT} \cos 2\phi_{pq} + h\sigma'_{LT} \sin\phi_{pq} \quad (12)$$

where the superscript on $\sigma^{\pm}$ refers to the helicity, ϕ_{pq} is the angle between the plane defined by the incoming and outgoing electron momenta and plane defined by the ejected proton and neutron, the ρ's depend only on the kinematics, f are the structure functions, c is proportional to the Mott cross section (see Equation 2), the σ's are the partial cross sections for each component, and h is the helicity of the electron beam (± 1). To extract A'_{LT} consider the asymmetry

$$A(\phi_{pq}) = \frac{\sigma^+ - \sigma^-}{\sigma^+ + \sigma^-} \quad (13)$$

where the superscripts refer to the helicity of the electron beam. Substituting Equation 12 into Equation 13 one obtains

$$A(\phi_{pq}) = \frac{\sigma^+ - \sigma^-}{\sigma^+ + \sigma^-} = \frac{\sigma'_{LT} \sin\phi_{pq}}{\sigma_L + \sigma_T + \sigma_{LT} cos\phi_{pq} + \sigma_{TT} \cos 2\phi_{pq}} \quad (14)$$

so for $\phi_{pq} = 90^\circ$ the asymmetry becomes

$$A(\phi_{pq} = 90^\circ) = A'_{LT} = \frac{\sigma_{90}^+ - \sigma_{90}^-}{\sigma_{90}^+ + \sigma_{90}^-} = \frac{\sigma'_{LT}}{\sigma_L + \sigma_T - \sigma_{TT}} \approx \frac{\sigma'_{LT}}{\sigma_L + \sigma_T} \quad (15)$$

The last approximation above will hold if σ_{TT} is small compared to σ_L or σ_T as has been observed [8, 12, 13].

Now consider taking the $\sin\phi_{pq}$ moment of the distribution for the two different choices of helicity.

$$\langle \sin\phi_{pq}\rangle_{\pm} = \frac{\int_0^{2\pi} \sigma^{\pm} \sin\phi_{pq} d\phi_{pq}}{\int_0^{2\pi} \sigma^{\pm} d\phi_{pq}} \tag{16}$$

$$= \frac{\int_0^{2\pi} (\sigma_L + \sigma_T + \sigma_{LT}\cos\phi_{pq} + \sigma_{TT}\cos 2\phi_{pq} + h\sigma'_{LT}\sin\phi_{pq}) \sin\phi_{pq} d\phi_{pq}}{\int_0^{2\pi} (\sigma_L + \sigma_T + \sigma_{LT}\cos\phi_{pq} + \sigma_{TT}\cos 2\phi_{pq} + h\sigma'_{LT}\sin\phi_{pq}) d\phi_{pq}} \tag{17}$$

By the orthogonality of sines and cosines all of the terms disappear except for the σ'_{LT} term in the numerator and the ϕ_{pq}-independent terms in the denominator. The result is

$$\langle \sin\phi_{pq}\rangle_{\pm} = \frac{\pm\sigma'_{LT}}{2(\sigma_L + \sigma_T)} \approx \pm\frac{A'_{LT}}{2} \tag{18}$$

where we have used Equation 6, $h = \pm 1$, and again neglected the contribution of σ_{TT}. To determine $\langle \sin\phi_{pq}\rangle_{\pm}$ for a given bin in Q^2 and θ^{cm}_{pq} or p_m from the data one uses

$$\langle \sin\phi_{pq}\rangle_{\pm} = \frac{1}{N_{\pm}} \sum_{i=1}^{N_{\pm}} \sin\phi_i \tag{19}$$

where the sum is over the ϕ_{pq} distribution of the data, i's refer to individual events, and $N_{\pm}$ refers to the number of events of each helicity.

In Equation 18, σ'_{LT} depends on θ^{cm}_{pq}, Q^2, p_m or θ^{cm}_{pq}, but as a function of one of those variables, say θ^{cm}_{pq}, one expects to see behavior like that shown in Figure 9 below. The curve for one helicity is the opposite

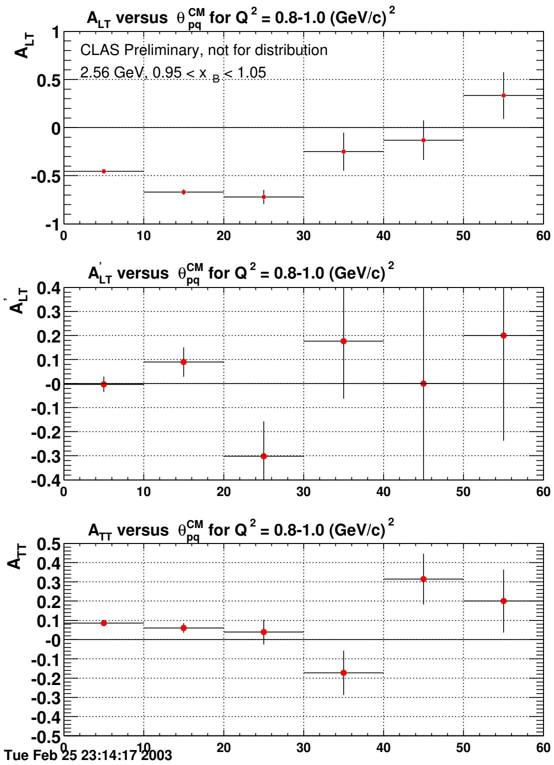

Figure 8: Asymmetries as a function of θ^{cm}_{pq} extracted using small angle bins.

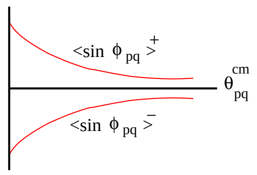

Figure 9: Schematic drawing showing the expected results for $\langle \sin\phi_{pq}\rangle^{\pm}$.

of the curve for the other helicity. However, acceptance effects can distort the expected distributions of Equation 18 if the CLAS acceptance has a component that varies as $\sin\phi_{pq}$. In such a case this component will survive the integration in Equation 17 when it is multiplying the constant portion of the cross section (σ_L and σ_T terms in Equation 17). Such an acceptance effect is additive and shifts $\langle\sin\phi_{pq}\rangle_{\pm}$ up or down, so

$$\langle\sin\phi_{pq}\rangle_{\pm}^{meas} = \pm\frac{\sigma'_{LT}}{2(\sigma_L+\sigma_T)} + \alpha \tag{20}$$

where α is the additive acceptance correction. See the Appendix for more details. If one has measured this $\sin\phi_{pq}$ moment for each helicity then the results can be combined so

$$\langle\sin\phi_{pq}\rangle_{+}^{meas} - \langle\sin\phi_{pq}\rangle_{-}^{meas} = \frac{\sigma'_{LT}}{\sigma_L+\sigma_T} \approx A'_{LT} \tag{21}$$

and

$$\frac{\langle\sin\phi_{pq}\rangle_{+}^{meas} + \langle\sin\phi_{pq}\rangle_{-}^{meas}}{2} = \alpha \qquad . \tag{22}$$

The asymmetry A'_{LT} is extracted with reduced sensitivity to acceptance corrections and the acceptance corrections have been measured from the data. This technique has been used by others for the $p(\vec{e},e'\pi^+)n$ and $p(\vec{e},e'p)\pi^0$ reactions [32, 33].

We have applied this analysis to our data and some preliminary results are shown in Figure 10. The two top panels show $\langle\sin\phi_{pq}\rangle_{+}^{meas}$ and $\langle\sin\phi_{pq}\rangle_{-}^{meas}$. The two distributions are not opposites of each other, implying there is a significant modification due to acceptance effects. The lower left panel shows the acceptance correction as a function of θ_{pq}^{cm} extracted by applying Equation 22. The acceptance correction α varies smoothly with θ_{pq}^{cm} and is in the range 4–12%. The lower right panel shows the asymmetry A'_{LT} determined by the difference between the two, helicity-dependent, $\sin\phi_{pq}$ distributions (see Equation 21). It reveals a significant, negative asymmetry at $\theta_{pq}^{cm} = 20-30^{\circ}$ that is 2–3 standard deviations away from zero. The asymmetry is consistent with zero in other θ_{pq}^{cm} bins within the measured uncertainty.

The two other asymmetries A_{LT} and A_{TT} can be extracted in a similar way. One can show that for A_{LT}

$$\langle\cos\phi_{pq}\rangle = = \frac{\int_0^{2\pi}\sigma^{\pm}\cos\phi_{pq}d\phi}{\int_0^{2\pi}\sigma^{\pm}d\phi_{pq}} \tag{23}$$

$$= \frac{\int_0^{2\pi}(\sigma_L+\sigma_T+\sigma_{LT}\cos\phi_{pq}+\sigma_{TT}\cos 2\phi_{pq}+h\sigma'_{LT}\sin\phi_{pq})\cos\phi_{pq}d\phi_{pq}}{\int_0^{2\pi}(\sigma_L+\sigma_T+\sigma_{LT}\cos\phi_{pq}+\sigma_{TT}\cos 2\phi_{pq}+h\sigma'_{LT}\sin\phi_{pq})d\phi_{pq}} \tag{24}$$

$$= \frac{\sigma_{LT}}{2(\sigma_L+\sigma_T)} \tag{25}$$

Combining the definition of A_{LT} (recall Equation 4) with Equation 12 for the cross section and neglecting the small transverse-transverse (TT) piece one obtains

$$\langle\cos\phi_{pq}\rangle \approx \frac{A_{LT}}{2} \qquad . \tag{26}$$

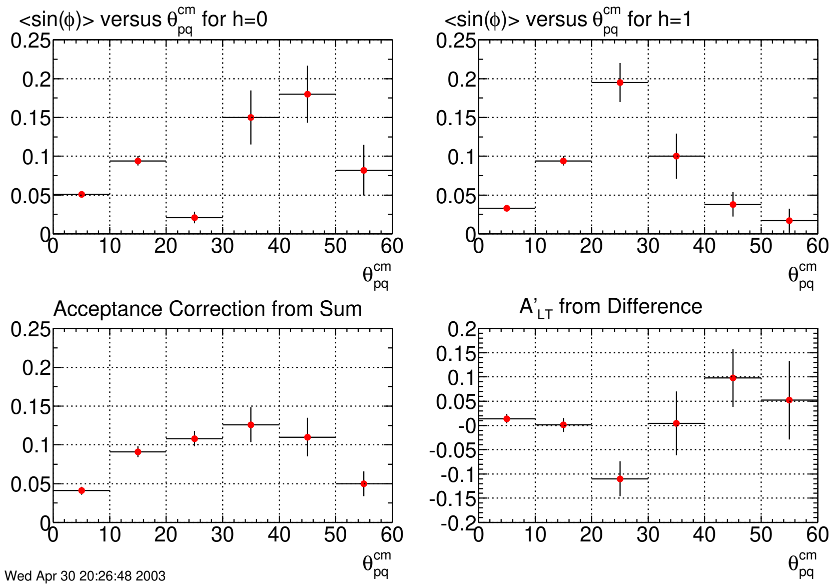

Figure 10: Preliminary results for $\langle \sin \phi_{pq} \rangle$ moments analysis for 2.56 GeV, normal field, not acceptance corrected, $0.8 < Q^2 < 1.0$ $(\mathrm{GeV/c})^2$, $0.95 < x_B < 1.05$. The notation is $h = 0$ for positive helicity and $h = 1$ for negative helicity.

Notice there is no dependence on helicity here. For A_{TT} one follows a similar procedure to show

$$\langle \cos 2\phi_{pq} \rangle = \frac{\int_0^{2\pi} \sigma^{\pm} \cos 2\phi_{pq} d\phi}{\int_0^{2\pi} \sigma^{\pm} d\phi_{pq}} = \frac{\sigma_{TT}}{2(\sigma_L + \sigma_T)} \approx \frac{A_{TT}}{2} \tag{27}$$

The figure below shows the asymmetries A_{LT} and A_{TT} extracted using the moments analysis and compared with the results using finite angle bins. The upper-left panel shows A_{LT} from the moments analysis and it reveals a large, negative asymmetry at $\theta_{pq}^{cm} = 0° - 30°$. This result is consistent with the finite-angle-bin measurement (lower-left panel), but has much better precision especially at large θ_{pq}^{cm}. The upper-right panel shows the results of the moment analysis for A_{TT}. There is a statistically significant positive asymmetry across the full angular range ($\theta_{pq}^{cm} = 0° - 60°$) for $\langle \cos 2\phi_{pq} \rangle$. There is good agreement with the finite-angle-bin analysis for the $0° - 10°$ bin and for $\theta_{pq}^{cm} = 30° - 50°$. In the intermediate angle bins the results differ, but the uncertainties on the finite-angle-bin results are large. It is worth noting here that we expect, based on previous results, that σ_{LT} and σ_{TT} will be small relative to σ_L and σ_T. The large asymmetries shown in Figure 11 include acceptance effects which have not yet been calculated so we can draw no conclusions yet about the true size of the acceptance-corrected asymmetries.

We investigated a third method for extracting A'_{LT} that takes advantage of the large acceptance of CLAS. Recall the expression for $A(\phi_{pq})$ (see Equation 14). The numerator in Equation 14 is proportional to $\sin(\phi_{pq})$ and the denominator is constant as long as σ_{LT} and σ_{TT} are small. If one forms the ratio of different helicities

$$A(\phi_{pq}) = \frac{\sigma^+ - \sigma^-}{\sigma + +\sigma^-} = \frac{N^+ - N^-}{N^+ + N^-} \frac{1}{A_Q} = \frac{\sigma'_{LT} \sin \phi_{pq}}{\sigma_L + \sigma_T + \sigma_{LT} cos\phi_{pq} + \sigma_{TT} \cos 2\phi_{pq}} \tag{28}$$

where A_Q is the beam charge asymmetry, then the distribution should have a sinusoidal dependence on ϕ if σ_{LT} and σ_{TT} are small relative to σ_T and σ_L. We have calculated this ratio and some preliminary results are shown in Figure 12 for four different angle bins in the range $Q^2 = 0.8 - 1.0$ $(\mathrm{GeV/c})^2$. The distributions were fitted with a sine curve and the results are shown on the figure. The fits all have acceptable reduced χ^2. We also tried fitting a more complex function that included the $\cos \phi_{pq}$ and $\cos 2\phi_{pq}$ terms in the denominator of Equation 28. We found the contributions from σ_{LT} and σ_{TT} were consistent with zero and there was no significant improvement to the fit.

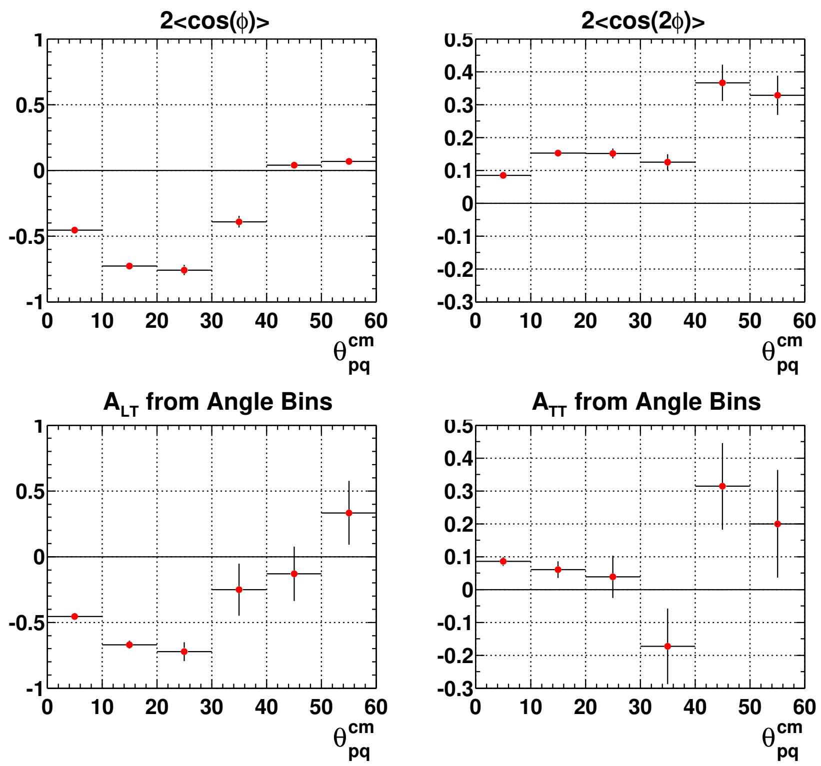

Figure 11: Comparison of A_{LT} and A_{TT} determined from an analysis of the ϕ moments of the distribution (upper panel) compared with the results from using small angle bins.

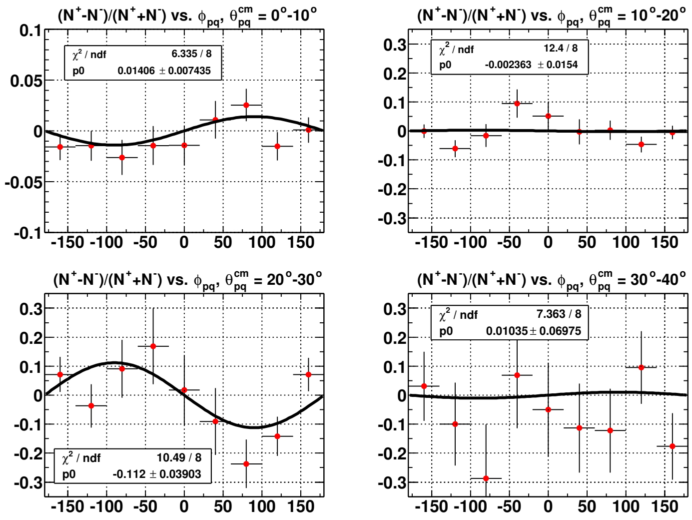

Figure 12: Preliminary results for ϕ dependence of A'_{LT} using the helicity ratio technique.

We compared the three different methods for measuring A'_{LT} and show the results in Figure 13. The top panel shows the angular distribution in θ_{pq}^{cm} measured using the $\sin\phi_{pq}$ moments of the distribution, the middle panel is from the fits to $A(\phi_{pq})$, and the bottom panel is from differences between small angle bins. It is worth noting again the first two methods take advantage of the large acceptance of CLAS while the

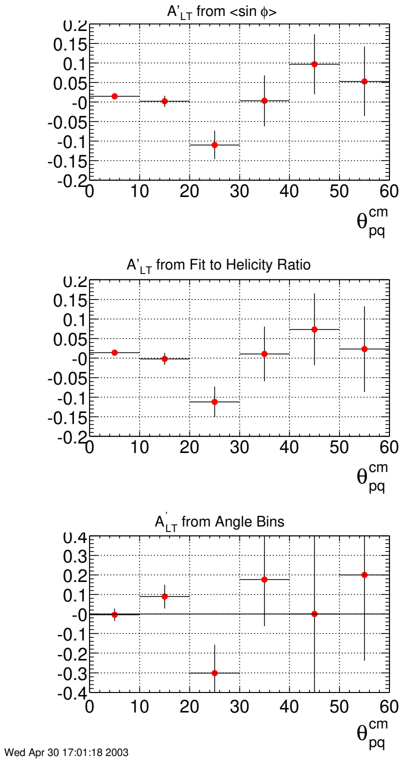

Figure 13: Comparison of A'_{LT} extracted using different analysis techniques. The calculation is not corrected for the CLAS acceptance.

last method ignores much of the data. The results in Figure 13 are for the range $Q^2 = 0.8 - 1.0$ (GeV/c)^2. The top two panels are very consistent with each other. The values of A'_{LT} in each angle bin agree for both methods as well as the size of the uncertainties in each angle bin. It is worth noting how A'_{LT} goes from small and positive for $\theta^{cm}_{pq} = 0° - 10°$ to large and negative for $\theta'_{pq} = 20° - 30°$. This is clearly seen in the shapes of the ϕ_{pq} distributions in Figure 12 in the upper-left and lower-left panels. We expect the $\sin\phi_{pq}$ moments and the $A(\phi_{pq})$ methods to be consistent; they represent the same quantity extracted from the same data set. The results in the bottom panel are consistent with the others within the uncertainties. We do not expect the results in the bottom panel to match as well since we are using a subset of the data which also means the uncertainties will be larger. We conclude that these methods are self-consistent and the $\sin\phi_{pq}$ moments analysis and the fit to $A(\phi_{pq})$ are equivalent methods. It is worth noting that the angular distribution shown here for $Q^2 = 0.8 - 1.0$ (GeV/c)^2 is a small fraction of the E5 data that covers the range $Q^2 = 0.2 - 5.0$ (GeV/c)^2.

There are other methods for checking our analysis. During the E5 run period the data were collected simultaneously from the proton target and will be compared with other CLAS analyses [32, 34]. The kinematic regions probed by the different E5 run conditions overlap each other so our results can be compared with different beam energies and/or torus magnet settings. As a final test of the quality of the analysis we make a preliminary comparison of our results with theory. In Figure 14 below we show A'_{LT} as function of θ^{cm}_{pq} calculated from the $\sin\phi_{pq}$ moments analysis along with a calculation from H. Arenhövel that includes relativistic effects, meson-exchange currents, isobar configurations, and final-state interactions [35]. The magnitude and sign of the asymmetry are reproduced by the calculation. However, the shape of the data is different; it is narrower and shifted to smaller angles. Note, this comparison is at $Q^2 = 0.8 - 1.0$ (GeV/c)^2 which is near the limit of validity of the Arenhövel calculation. These differences hint at the need for improvements to the hadronic model of nuclear physics.

We have begun to address the sources of uncertainty in our investigation. The CLAS has a finite

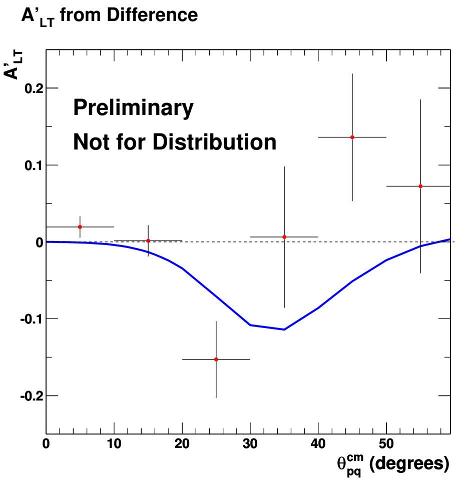

Figure 14: Comparison of results for A'_{LT} at 2.56 GeV, normal field, $0.8 < Q^2 < 1.0$ $(\mathrm{GeV/c})^2$, $0.95 < x_B < 1.05$ (not acceptance corrected). The measured asymmetry is corrected for the beam polarization. The blue curve is a calculation by Arenhövel.

angular resolution which becomes more important for small θ^{cm}_{pq}, *i.e.* when the emitted proton is moving nearly parallel to the 3-momentum transfer. In the limit of $\theta^{cm}_{pq} = 0$, the azimuthal angle, ϕ_{pq} is undefined. At small θ^{cm}_{pq} our determination of ϕ_{pq} will become unreliable because of this angular resolution. We have examined this 'pointing' error using the elastic scattering off the proton with the hydrogen target. We extracted the difference between the measured proton momentum and the 3-momentum transfer determined by incoming and outgoing electron momenta. The width of the distribution is about $\sigma \approx 0.6°$ and is symmetric about the origin. We will address this question along with other sources of uncertainty including the acceptance calculations as the project progresses.

Much work remains. We are not yet applying the corrections to remove the distortions of the data caused by CLAS such as momentum corrections, energy loss, corrections, *etc.* We are also improving data selection. Fiducial cuts on the electron and proton to define the active volume of the CLAS are being developed. Calculation of the acceptance of CLAS is just beginning. This step is critical for understanding the f_{LT} and f_{TT} results. It is less important for the f'_{LT} analysis because using the ratio of different helicities to calculate A'_{LT} reduces many of the systematic uncertainties. We have only begun investigating the sources of uncertainty in our analysis. The 'pointing' error described above and radiative corrections are two examples.

5 Conclusions

We propose to extract the structure functions f_{LT}, f_{TT}, and f'_{LT} of the deuteron in the region $Q^2 = 0.2 - 5.0$ $(\mathrm{GeV/c})^2$ using out-of-plane measurements recorded during the E5 running period. These data will challenge the existing 'standard model' of nuclear physics in a transition region in Q^2 where many expect the model to begin to break down and quark and gluon degrees of freedom to manifest themselves. More specifically, these data will test our understanding of relativistic corrections, meson-exchange currents, isobar configurations, and final-state interactions.

Our preliminary analysis of the data from the E5 running period shows that we can extract the structure functions with good to excellent precision. We have found this can be done using the different azimuthal moments of the data: $\langle \cos\phi_{pq} \rangle$ for f_{LT}, $\langle \cos 2\phi_{pq} \rangle$ for f_{TT}, and $\langle \sin\phi_{pq} \rangle$ for f'_{LT}. The fifth structure function f'_{LT} can be extracted from the moment analysis and also from fitting the A_ϕ asymmetry. Both methods give equivalent results. This last structure function is small and likely the most difficult to measure so it provides a stringent test of our techniques. Our preliminary results show that asymmetries as large as 0.15 can be expected for f'_{LT}. The statistical uncertainties range in size from 0.01 at small θ^{cm}_{pq} to 0.04 at $\theta^{cm}_{pq} \approx 30°$.

The results shown here for f'_{LT} represent only a small fraction of the total data set.

References

[1] PAC 14 Few-Body Workshop, Williamsburg, VA, July, 1998.

[2] S.Jeschonnek, Phys. Rev **C63** 034609 (2001).

[3] S.Jeschonnek and T.W.Donnelly, Phys. Rev. **C57** 2438 (1998).

[4] S.Jeschonnek and J.W.Van Orden, Phys. Rev. **C62** 044613 (2000).

[5] F.Ritz, H.Goller, Th. Wilbois, and H.Arenhövel, Phys. Rev. **C55**, 2214 (1997).

[6] R.Gilman and F.Gross, J.Phys.G: Nucl. Part. Phys. **28**, R37 (2002).

[7] 'Opportunities in Nuclear Science: A Long-Range Plan for the Next Decade', DOE/NSF Nuclear Science Advisory Committee, April 2002, p. 30.

[8] S.Gilad, W.Bertozzi, and Z.-L.Zhou, Nucl. Phys. **A631** 276c (1998).

[9] S. Boffi, C. Giusti, F. D. Pacati, and M. Radici, *Electromagnetic Response of Atomic Nuclei*, Oxford University Press, Oxford, England, 1996.

[10] S.M.Dolfini *et al.*, Phys. Rev. **C60** 064622 (1999).

[11] S.M.Dolfini, *et al.*, Phys. Rev. **C51** 3479 (1995).

[12] T.Tamae, *et al.*, Phys. Rev. Lett. **59** 2919 (1987).

[13] M. van der Schaar *et al.*, Phys. Rev. Lett. **68**, 776 (1992).

[14] H.J.Bulten, *et al.*, Phys. Rev. Lett. **74** 4775 (1995).

[15] E.Hummel and J.A.Tjon, Phys. Rev. Lett. **63**, 1788 (1989); Phys. Rev. **C42** 423, (1990).

[16] H.Arenhövel, Nucl. Phys. **A365**, 349 (1981).

[17] W.Fabian and H.Arenhövel, Nucl. Phys. **A314**, 252 (1979).

[18] D.Jordan *et al.*, Phys. Rev. Lett. **76** 1579 (1996).

[19] J.E.Ducret, *et al.*, Phys. Rev. **C49** 1783 (1994).

[20] F.Frommberger, *et al.* Phys. Lett. **B339** 17 (1994).

[21] P.E.Ulmer, *et al.*, Phys. Rev. Lett. **89**, 062301, 2002.

[22] H.Arenhövel, W.Leidemann and E.L.Tomusiak, Phys. Rev. **C52**, 1232 (1995).

[23] Z.-L. Zhou *et al.*, Phys. Rev. Lett. **87** 172301 (2001).

[24] C.Hadjidakis, private communication.

[25] J.Lachniet, 'Report on momentum corrections in E5', http://clasweb.jlab.org/cgi-bin/ENOTE/enote.pl?nb=e5&action=view&page=109, [Accessed 10 July, 2003].

[26] J.Lachniet, 'A second look at momentum corrections', http://clasweb.jlab.org/cgi-bin/ENOTE/enote.pl?nb=e5&action=view&page=166, [Accessed 10 July, 2003].

[27] M.Anghinolfi, CLAS-Note 2001-020.

[28] A.Afanasev, I.Akushevich, V.Burkert, and K.Joo, Phys.Rev., **D66**, 074004, 2002.

[29] L.W.Mo and Y.S.Tsai, Rev. Mod. Phys., **41**, 205, 1969.

[30] J.Schwinger, Phys. Rev., **76**, 898, 1949.

[31] Juan Cornejo, *radiative corrections, external and internal bremsstrahlung factors*, Retrieved on January 30, 2003 from http://www.calstatela.edu/academic/nuclear_physics/schwin12_extbrems.html.

[32] K.Joo and C.Smith, CLAS Analysis Note 2001-009.

[33] H.Avakian, CLAS Analysis Note 2002-101.

[34] K.Joo and C.Smith, private communication.

[35] H.Arenhövel, private communication.

A Appendix

A.1 Radiative Corrections

To test our modifications to EXCLURAD we will compare them with the more traditional approaches. Below we describe how to relate the parameters of the Schwinger-style calculation with the approach used in EXCLURAD. In the Schwinger method one calculates the radiative correction for the scattering of an electron in a Coulomb field. This corresponds to inclusive electron scattering. An essential step in the calculation is to integrate over the radiative tail of the energy of a scattered electron to arrive at a correction factor for the yield lost to the emission of photons. The parameters of that integration are defined in Figure 15 [31]. The parameter ΔE is the energy range over which the integral is performed (starting at the

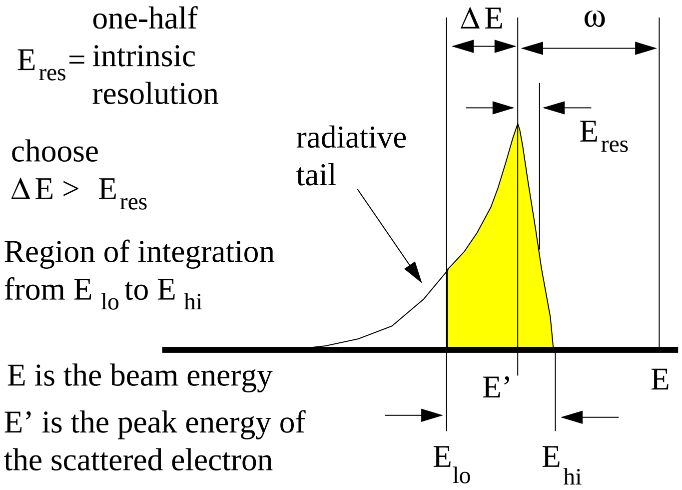

Figure 15: Energy spectrum of scattered electron showing definitions of quantities used in Schwinger radiative correction calculation.

unradiated energy of the electron) to estimate the yield lost to radiated photons.

Afanasev, *at al.* follow an analogous procedure in their more sophisticated approach [28]. They integrate over the radiative tail of the scattered electron, but they perform the integration in terms of the covariant 'inelasticity' v defined as

$$v = \Lambda^2 - m_u^2 \tag{29}$$

where m_u is the mass of the undetected hadron and Λ is the four-momentum of the missing or undetected particles. The quantity v describes the missing mass due to the emission of a bremsstrahlung photon and can be rewritten as

$$v = W^2 + m_h^2 - m_u^2 - 2WE_h \tag{30}$$

where W is the mass of the system recoiling against the electron, m_h is the mass of the detected hadron, and E_h is the center-of-mass energy of the detected hadron. To determine the relationship between ΔE and v consider the usual expression for W^2

$$W^2 = M^2 + 2M(E - E') - Q^2 \tag{31}$$

where

$$Q^2 \approx 4EE' \sin^2 \frac{\theta}{2} \tag{32}$$

M is the target mass, and θ is the electron scattering angle. However, for an event with a radiated photon, the measured energy of the scattered electron is not E', but some lower energy

$$E_{lo} = E' - \Delta E \tag{33}$$

so W for this event will not be 'correct'. The new value of W is

$$W_{rad}^2 = M^2 + 2M(E - E_{lo}) - 4EE_{lo} \sin^2 \frac{\theta}{2} \tag{34}$$

Using Equations 33 and 34 in the expression for v in Equation 30 one obtains the following function of ΔE.

$$\begin{aligned} v = {} & M^2 + 2M(E - E' + \Delta E) - 4E(E' + \Delta E) \sin^2 \frac{\theta}{2} \\ & + m_h^2 - m_u^2 - 2E_h \sqrt{M^2 + 2M(E - E' + \Delta E) - 4E(E' + \Delta E) \sin^2 \frac{\theta}{2}} \end{aligned} \tag{35}$$

This expression can be re-arranged so

$$v = W_0^2 + m_h^2 - m_u^2 + 2\Delta E(M + 2E \sin^2 \frac{\theta}{2}) - 2E_h \sqrt{W_0^2 + 2\Delta E(M + 2E \sin^2 \frac{\theta}{2})} \tag{36}$$

where

$$W_0^2 = M^2 + 2M(E - E') - 4EE' \sin^2 \frac{\theta}{2} \tag{37}$$

and the quantities E, E', and θ are determined by the electron kinematics. The hadron energy E_h is determined by the choice of the angle of the outgoing hadron relative to $\vec{q}$, the three-vector of the momentum transfer. The masses M, m_h, and m_u are all known.

As an example of applying Equation 35 consider the following kinematics. The results of the calculation

$E = 2.558$ GeV	$E' = 2.345$ GeV	$\theta = 14.84°$
$m_h = 0.938$ GeV	$m_u = 0.940$ GeV	$\theta_h^{cm} = 45°$
$M = 1.876$ GeV	$Q^2 = 0.52$ (GeV$/c)^2$	$W = 1.93$ GeV

Table 1: Kinematics for calculating $v(\Delta E)$.

are shown in Figure 6. The dependence of v on ΔE is almost linear implying the importance of that term in Equation 36 over the sum of all the other terms.

A.2 Acceptance Effects in $\langle \sin \phi_{pq} \rangle_\pm$

To more clearly understand Equation 20 which relates $\langle \sin \phi_{pq} \rangle_\pm$ to A'_{LT} and the acceptance recall again the expression for the differential cross section for $d(\vec{e}, e'p)n$.

$$\frac{d^3\sigma}{d\nu d\Omega_e d\Omega_p} = \sigma^\pm = c[\rho_L f_L + \rho_T f_T + \rho_{LT} f_{LT} \cos(\phi_{pq}) + \rho_{TT} f_{TT} \cos(2\phi_{pq}) + h\rho'_{LT} f'_{LT} \sin(\phi_{pq})] \tag{38}$$

$$= \sigma_L + \sigma_T + \sigma_{LT} \cos \phi_{pq} + \sigma_{TT} \cos 2\phi_{pq} + h\sigma'_{LT} \sin \phi_{pq} \tag{39}$$

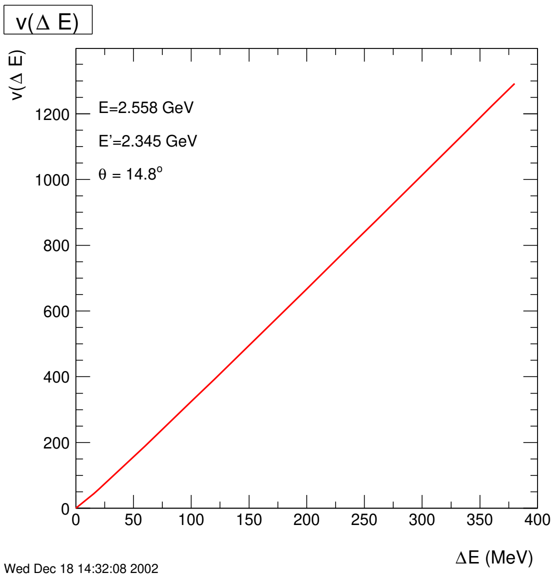

Figure 16: Dependence of v on ΔE for the kinematics listed in Table 1.

The $\sin\phi_{pq}$ moment of the data at a given Q^2 and θ_{pq}^{cm} or p_m is defined by the following expression.

$$\langle \sin\phi_{pq}\rangle_{\pm} = \frac{\int_0^{2\pi} \sigma^{\pm} \sin\phi_{pq} d\phi}{\int_0^{2\pi} \sigma^{\pm} d\phi} \tag{40}$$

Now let

$$\sigma^{\pm} = \kappa\epsilon(\phi_{pq})N^{\pm}(\phi_{pq}) \tag{41}$$

where $N^{\pm}$ is the number of counts for each helicity, ϵ is the CLAS acceptance and may vary with ϕ_{pq}, and κ contains all the other helicity-independent, kinematic factors needed to determine cross sections. In turn, $N^{\pm}$ is composed of different longitudinal and transverse components so

$$N^{\pm}(\phi_{pq}) = N_L^{\pm} + N_T^{\pm} + N_{LT}^{\pm}\cos\phi_{pq} + N_{TT}^{\pm}\cos 2\phi_{pq} + hN_{LT}^{\pm\,\prime}\sin\phi_{pq} \qquad . \tag{42}$$

Hereafter, we will suppress the $\pm$ superscript for clarity and it will be assumed that all $N's$ depend on the helicity. Finally, the CLAS acceptance as a function of ϕ_{pq} at a given Q^2 and θ_{pq}^{cm} or p_m can be expressed as

$$\epsilon(\phi_{pq}) = A_0 + \sum_{m=1}^{\infty}(a_m \sin m\phi_{pq} + b_m \cos m\phi_{pq}) \tag{43}$$

where we have taken advantage of the completeness of the sines and cosines. We expect any ϕ_{pq} dependence in the CLAS acceptance to vary slowly so we approximate it by taking the sum in Equation 43 up to $m = 2$ so

$$\epsilon(\phi_{pq}) = A_0 + a_1\sin\phi_{pq} + b_1\cos\phi_{pq} + a_2\sin 2\phi_{pq} + b_2\cos 2\phi_{pq} \qquad . \tag{44}$$

Substituting Equations 41, 42, and 44 into Equation 40 one obtains (after doing some algebra and some integrals) the following expression

$$\langle \sin\phi_{pq}\rangle^{\pm} = \frac{(N_L + N_T - \frac{N_{TT}}{2})a_1 + \frac{N_{LT}a_2}{2} \pm N'_{LT}A_0}{2(N_L + N_T)A_0 + N_{LT}b_1 + N_{TT}b_2 + N'_{LT}a_1} \tag{45}$$

where we have used $h = \pm 1$. In the numerator, N_{TT} and N_{LT} are both much less than $N_L + N_T$ so we can neglect their contribution. We retain the N'_{LT} term since since it will survive when we take the difference between the moments for the positive and negative helicities (the N_{TT} and N_{LT} terms will cancel in the difference). In the denominator, we can apply the same reasoning and neglect the N_{LT} and N_{TT} terms. Here we can also neglect the N'_{LT} term because it will have a small effect on the final difference. The result is

$$\langle \sin \phi_{pq} \rangle^{\pm} = \frac{(N_L + N_T)a_1 + N'_{LT} A_0}{2(N_L + N_T)A_0} \tag{46}$$

$$= \frac{a_1}{2A_0} + \frac{N'}{2(N_L + N_T)} \tag{47}$$

$$= \alpha + \frac{\sigma'_{LT}}{2(\sigma_L + \sigma_T)} \tag{48}$$

which is the form of Equation 20. We have used Equation 41 to eliminate the N's and labeled the first term α to be consistent with the text.